Parallax error in the head-direction system indicates simple cue-anchoring mechanism

Sven Krausse
Forschungszentrum Jülich - PGI 15
RWTH Aachen University - Institute for Electrical Engineering and Information Technology
Aachen, Germany
s.krausse@fz-juelich.de

Adrian J. Duszkiewicz
Division of Psychology, University of Stirling
Stirling, United Kingdom

Emre Neftci
Forschungszentrum Jülich - PGI 15
RWTH Aachen University - Institute for Electrical Engineering and Information Technology
Aachen, Germany

Friedrich T. Sommer
UC Berkeley - Redwood Center for Theoretical Neuroscience
Berkeley, USA

Alpha Renner
Forschungszentrum Jülich - PGI 15
Aachen, Germany
a.renner@fz-juelich.de

Abstract

Spatial navigation relies on the head-direction (HD) system, which integrates angular head velocity (AHV) to track orientation. Since integration accumulates drift over time, visual landmarks provide corrective cues. However, such sensory cues are perceived egocentrically and must therefore be transformed into allocentric coordinates. The parallax effect, where nearby objects appear to shift more than distant ones during movement, should lead to a systematic position-dependent HD error unless there is a correction mechanism. How the HD system solves this problem remained an open question. Here, we analyzed postsubicular HD cell activity in mice navigating in a restricted environment with a single visual cue. We discovered a systematic parallax bias in the decoded HD, indicating that the HD system misinterprets the cue's position depending on the viewing angle. The observed error was smaller than predicted by a pure vision model, which can be explained by the combination of AHV integration with simple visual anchoring. In less restricted experimental settings with multiple cues available, the parallax effect is drastically decreased. These experimental findings indicate that the HD system does not actively correct for parallax in a position-dependent manner, but instead relies on a simple cue anchoring mechanism for the transformation of the egocentrically observed cues into an allocentric reference frame. The use of AHV integration and multiple cues is sufficient to account for parallax and produce a stable HD signal for spatial navigation. This sheds light on the mechanisms of ego-to-allocentric transformation in neural systems, which is crucial for the formation of the cognitive map. Furthermore, it highlights a fundamental trade-off in neural coding between computational efficiency and positional accuracy, with implications for biological and artificial navigation systems.

Keywords: navigation; postsubiculum; parallax; sensory integration; head-direction cells; bearing cells; landmark anchoring

Introduction

Accurate spatial navigation depends on a reliable sense of direction, which is provided by the head-direction (HD) cell network. HD cells, discovered in many brain areas, including the postsubiculum (PoSub) (Rank, 1984; J. Taube et al., 1990), thalamic nuclei (LDN, AdN, Mizumori & Williams (1993); J. S. Taube (1995)), hypothalamus (LMN, Stackman & Taube (1998)), and entorhinal cortex (Giocomo et al., 2014), encode the animal's allocentric (north, east, west, south) orientation, effectively serving as an internal neural compass. The HD cell network receives input from angular head velocity (AHV) cells, which signal changes in the head direction and enable the HD network to integrate velocity over time (McNaughton et al., 1991, 2006; J. S. Taube, 2007). The HD system is typically modeled as a set of continuous ring attractors (Skaggs et al., 1994; Zhang, 1996; Redish et al., 1996; Chaudhuri et al., 2019; Bicanski & Burgess, 2016). LMN and

AdN are believed to be primarily involved in the AHV integration process, projecting the integrated HD state to the Postsubiculum (Zhang, 1996; Hahnloser, 2003; Boucheny et al., 2005; Bicanski & Burgess, 2016).

Visual landmark cues play a crucial role in anchoring the HD system to stable reference points in the environment (J. S. Taube et al., 1990; Goodridge et al., 1998; Knierim et al., 1995; Zugaro, Berthoz, & Wiener, 2001). Empirical studies have demonstrated that HD cells align their preferred firing direction (PFD) with distal visual landmarks (J. S. Taube et al., 1990; Zugaro et al., 2003). However, visual (and other sensory) landmark observations are inherently egocentric and must first be transformed to an allocentric representation. Neural circuits in the retrosplenial cortex (RSC) and PoSub are believed to be crucial in this transformation, as RSC encodes landmark distance and angle information in so-called bearing cells (Alexander et al., 2020; Bicanski & Burgess, 2020) and directly projects onto PoSub.

Previous models have suggested a learning mechanism between bearing and HD cells that is responsible for this egocentric-to-allocentric transformation (Skaggs et al., 1994; Zhang, 1996; Hahnloser, 2003; Bicanski & Burgess, 2016; Boucheny et al., 2005). However, the mapping between egocentric bearing angles and allocentric head direction is position dependent, as an object's bearing angle changes when the observer moves relative to it. This effect is known as the parallax effect. Previous models have assumed (sometimes implicitly) that anchoring cues are positioned effectively at infinite distance, thereby removing the parallax effect (Skaggs et al., 1994; Zhang, 1996; Hahnloser, 2003; Boucheny et al., 2005). Other models have suggested explicit position-dependent correction mechanisms through hippocampal place cells (Bicanski & Burgess, 2016). However, such a correction mechanism introduces a circular dependence, as place cells (and other allocentric spatial estimates, such as grid cells in the MEC) are believed to utilize an already existing stable HD signal to update their position estimate using path integration (McNaughton et al., 2006; Burak & Fiete, 2009). Indeed, developmental studies have suggested that the HD system produces stable HD cells even before place cells and grid cells emerge in the hippocampal formation (Tan et al., 2017). Furthermore, lesion studies in mice showed that a stable HD signal in the PoSub is maintained and stable after lesioning the hippocampus (Golob & Taube, 1997).

Thus, we arrive at the following dilemma: How is the HD system anchored to (finite distant) landmarks in the environment without introducing parallax error to the HD estimation? In this work, we present findings that in highly restricted environments with only a single cue, we can, in fact, measure a position-dependent error in HD cells in the PoSub, indicating that the HD cell network is subject to the parallax effect and may not actively correct for it. The detected parallax error is smaller than expected from a purely vision-based model, which can be partly explained through the use of AHV integration. Analysis of a second dataset in a less restricted environment additionally shows that the parallax error effectively vanishes when more cues are available. This suggests that the use of multiple cues allows for the suppression of the parallax error through averaging estimates. Simulations of this 'multi-cue' setting confirm that this mechanism indeed removes the parallax error.

Overall, our findings suggest that the HD cell network employs a simple cue-anchoring strategy without active position-dependent correction mechanisms. Instead, the system relies on AHV integration and the use of multiple cues to correct for the parallax effect, producing a stable HD signal for spatial navigation. Finally, we propose a HD formation model that synthesizes our experimental findings with previous theories, demonstrating how the combination of AHV integration and multi-cue averaging can effectively anchor the HD signal to maintain a stable orientation in the physical world.

Results

The HD system shows a parallax error in a single-cue environment

We first investigated whether we observed a parallax effect in the mouse head-direction (HD) cells in the postsubiculum (PoSub) in a single cue environment. To this end, we analyzed data of eleven sessions from ten mice freely navigating a circular platform within a square box (dataset partially published previously in Duszkiewicz et al. (2024), see Methods). Crucially, the environment consisted of a dark enclosure with only a single active LED cue at one of the walls, eliminating any other possible visual landmarks (e.g., corners of the square box). Each recording session consisted of multiple trials, where the cue position was changed between each trial, alternating between two sides of the wall. In six out of the eleven sessions, the cue rotation led to a remapping of the decoded HD, shifting it by $90°$. Unless otherwise specified, we reoriented the position data for these cases in each trial such that the cue was effectively always positioned at the north wall (Fig. 1c). In sessions without remapping, we constrained the analysis to the trials with the original cue to restrict the analysis to time periods where the animal is consistently perceiving the same cue. We discuss the influence of the switching cue in a later section (Inferring the Anchoring Angle from Parallax).

Based on the recorded spiking activity and the animals tracked HD α_{true} we decoded the internal head direction signal α_{dec} using a Bayesian decoder (Fig. 1a, Methods). We then computed the decoding error β_{dec} as the difference between the decoded and tracked HD:

$$\beta_{\text{dec}} = \alpha_{\text{dec}} - \alpha_{\text{true}}.^{1} \tag{1}$$

Suppose the HD network employs a simple cue-anchoring technique. In that case, we expect a systematic difference between the decoded and tracked HD that depends on the

[1] For readability, we omit the wrapping of angles from the equations. In practice, whenever we took sums or differences of angular measurements, we applied a wrapping function $f(x) = \arg(e^{ix})$ to the result of the addition/subtraction.

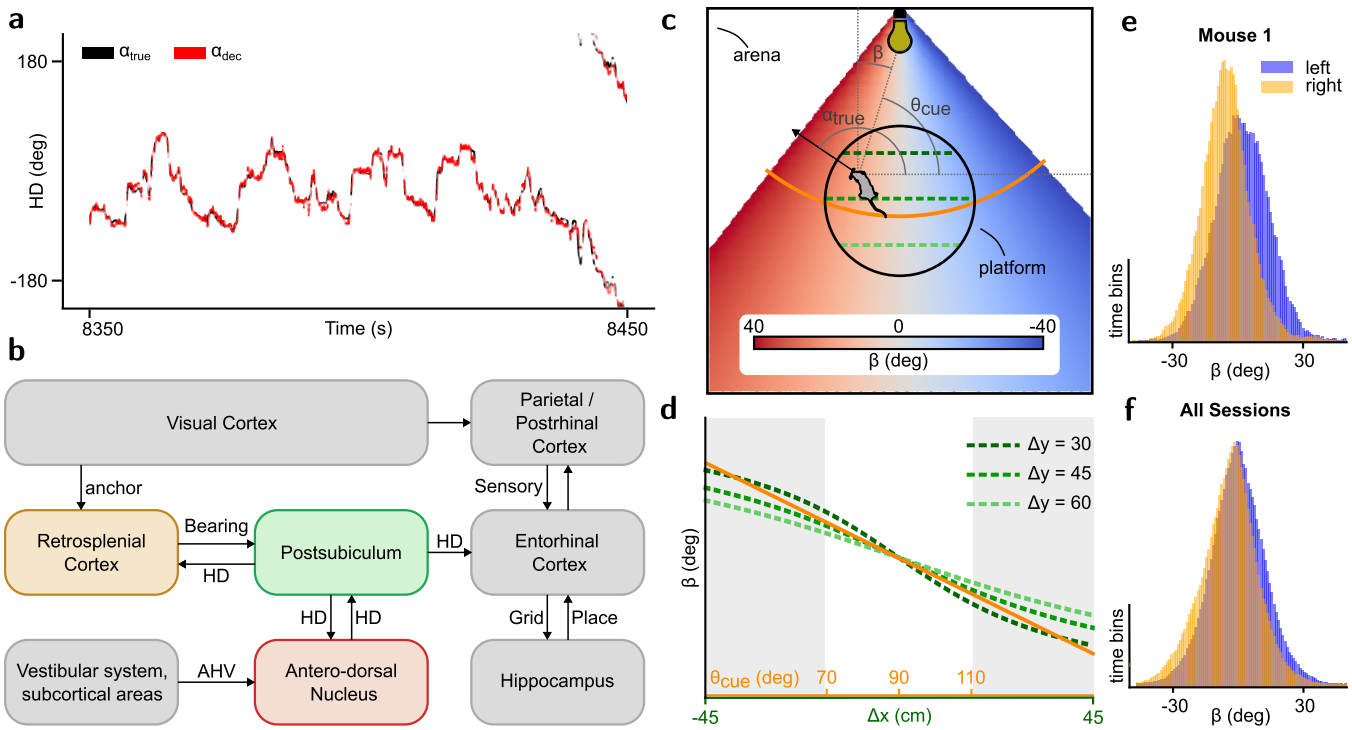

Figure 1: **Illustration of position-dependent parallax error in head direction (HD) estimation.** (**a**) Arbitrary example data from Duszkiewicz et al. (2024) showing the true head direction and the decoded head direction. The difference between these two curves β_{dec} is used for the linear regression in Eq. 5. (**b**) Illustration of functional connectivity in the HD circuit after Hulse & Jayaraman (2020); J. S. Taube (2007). (**C**) Parallax-induced error β color-coded at different locations in the arena. The four colored lines through the arena are the trajectories along which the error is plotted in panel E. (**d**) Parallax-induced error β as a function of lateral displacement Δx for three different distances Δy from the cue. Distances are also shown in panel C. The error is not linearly dependent on $\Delta x(t)$ but rather on $\theta_{cue}(t)$ (orange line). We, therefore, perform the linear regression using this angle. (**e**) Histogram of measured decoding errors β_{dec} in a single recording session. The two histograms correspond to time points where the animal is either on the left (blue) or right (orange) side of the circular platform. (**f**) Same as (e), aggregated over all six recording sessions.

animal's relative position to the cue due to the parallax effect (Fig. 1c,d). As a first indication, we split the recording data into two subsets where the animal was either on the left or right side of the platform and compared the resulting distributions of decoding errors for each subset (Fig. 1e,f). All eleven sessions exhibited highly significant differences in mean decoding errors between left and right platform positions (Welch's t-tests, all $p < 0.001$; see Suppl. Tab. 1). In 10 of 11 sessions, animals showed consistently higher decoding errors when positioned on the left side of the platform compared to the right side (Cohen's $d = 0.13$ to 1.16, median $|d| = 0.34$). When the animals were on the right side of the platform, we observed a shift towards negative β_{dec} values; when they were on the left side, there was a shift to positive β_{dec} values.

This observation qualitatively matches the hypothesis of parallax errors in the HD network. To quantify the amount of parallax in each session, we next derived the expected amount of parallax in a purely visually guided scenario. We then compared this expectation to the measured decoding error.

Quantifying the parallax error

In a simple cue anchoring model, there exists a fixed mapping between the egocentric viewing angle of the cue ϕ_{cue} and the vision based HD estimate α_{vis} that is defined by the anchoring angle γ_{anchor}:

$$\alpha_{vis}(t) = \gamma_{anchor} - \phi_{cue}(t). \tag{2}$$

The egocentric viewing angle ϕ_{cue} is defined as the difference between the true head direction α_{true} and the allocentric cue angle θ_{cue} (that is, the angle of the vector pointing from the animal to the cue):

$$\phi_{cue}(t) = \theta_{cue}(t) - \alpha_{true}(t). \tag{3}$$

Substituting Eq. 3 in Eq. 2, we obtain a linear relationship (up to the angular periodicity) between the decoding error β_{vis} and the position dependent allocentric cue angle θ_{cue} (Fig.1c,d.):

$$\begin{aligned} \beta_{vis}(t) &= \alpha_{vis}(t) - \alpha_{true}(t) \\ &= \gamma_{anchor} - \theta_{cue}(t). \end{aligned} \tag{4}$$

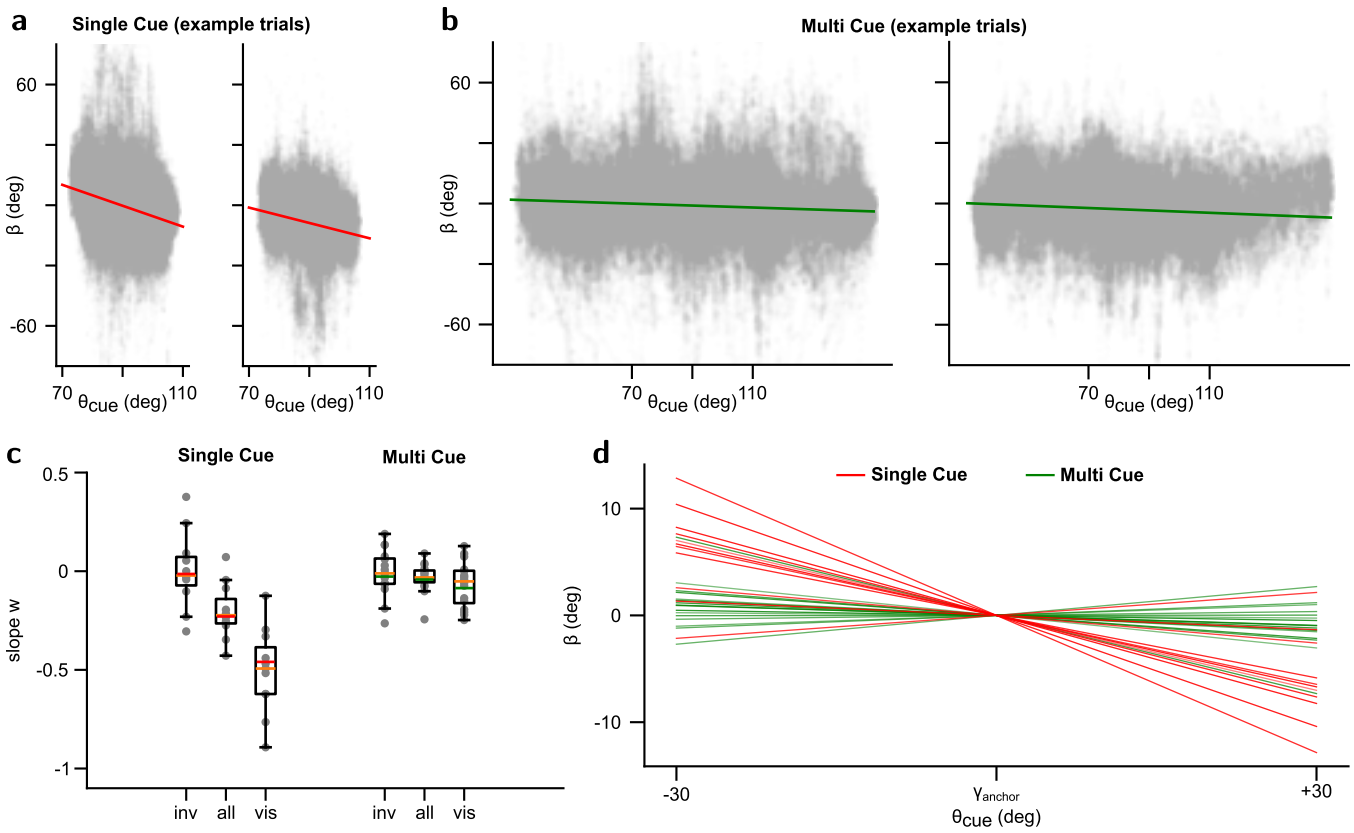

Figure 2: **Quantification of the parallax-induced error in head direction (HD) estimation across different recording sessions. (a,b):** Example sessions linear regression results. Each panel shows the relationship between the allocentric angle of the vector from the animal to the cue θ_{cue} and the observed angular error β_{dec} as in Eq. 5. Individual data points are calculated from the decoded HD traces, colored lines indicate the fitted linear model. The range of θ_{cue} is determined by the size of the environment. **(a):** Single-cue experiment results for two example sessions. **(b):** Multi-cue experiment results for two example session where the animal was freely navigating an illuminated square arena with a cue card on one of the walls. **(c):** Box plots for all measured slopes for the two experimental setups. For each session, the slopes are fitted for periods when the cue is behind the animal (inv - invisible), for all data points (all), and for periods when the cue is in front of the animal (vis - visible). Orange markers indicate the median slope in each box plot, red/green colored markers indicate the weighted mean slope. **(d):** All fitted slopes for the three datasets. To make the slopes visually better comparable, the fitted lines are aligned to have the same x-intercept, effectively aligning the fitted lines on their respective anchoring angles γ_{cue}.

To test whether this decoding error relation is also detectable in experimental data, we used the decoded error β_{dec} (Eq.1) of the eleven mice and also computed the allocentric cue angle $\theta_{cue}(t)$ from the animals' tracked position. We then performed a bootstrapped linear regression:

$$\beta_{dec}(t) = w \cdot \theta_{cue} + b + \varepsilon(t), \tag{5}$$

where the slope w and intercept b are fitted parameters minimizing the squared error of the linear fit to the observed data points. ε is the residual (Methods).

Eq. 5 corresponds to Eq 4 where the slope is $w = -1$ and the intercept $b = -w \cdot \gamma_{anchor}$. Note that the linear regression fits the y-intercept, while the anchoring angle is the x-intercept. A purely vision-based head direction signal would therefore predict a slope of $w = -1$ (full parallax-error) and an x-intercept corresponding to the specific cue's anchoring angle γ_{anchor}.

We assume that each cue and each animal has a distinct anchoring angle. Therefore, the fit was performed separately for each session (Fig. 2a). We observed fitted slopes w significantly below 0 for ten out of eleven recording sessions (weighted mean slope $\overline{w} = -0.23 \pm 0.008$), meaning that the parallax error can be observed in all but one sessions (bootstrapped t-test, p-values < 0.05, Methods, Suppl. Tab. 3). However, the maximal negative measured slope was -0.43, indicating a lower position dependence of the decoding error than predicted by a pure vision model (where we would expect a slope of -1). Furthermore, the relatively low R^2 values (range: $0.001 - 0.127$, see Suppl. Tab. 3) suggest that additional factors influence HD decoding errors. One essential and well-known additional factor is AHV integration, which we examine in the next section.

Attenuated parallax through AHV integration

The need for AHV integration is most evident when the mouse fails to see the cue. To obtain an HD estimate even in such cases, the animal naturally has to integrate its previous state and cannot rely on visual cues alone. A lower parallax can be assumed in such cases because the cue angle θ_{cue} can change when the mouse walks around while the cue is invisible. During these periods, the last seen parallax error is roughly maintained, reducing the slope in these periods. Vice versa, the amount of parallax should be higher during periods where the animal is directly facing the cue, as it is more likely for the visual input to influence the current HD estimation.

We therefore also investigate whether parallax remains when the cue is invisible. Fig. 2c indeed shows a tendency towards lower parallax error when the cue is behind the mouse (and can therefore be assumed invisible). Ten out of eleven sessions show a significantly lower slope in periods where the cue is invisible (Suppl. Tab. 3). When the animal is facing the cue directly, the inverse is true, and the amount of parallax error increases; that is, the fitted slope w approaches -1. Testing the distributions of measured slopes in the invisible, all, and visible conditions, we find that all three significantly differ (t-test p-value < 0.05, 2c, Suppl. Tab. 2). The variability in the amount of parallax strongly suggests that AHV integration acts as one mechanism to attenuate the parallax effect, which can also be observed in the simulations introduced below.

A second factor that could attenuate parallax is the use of multiple cues in the environment. In such a setting, the HD errors introduced for each cue could average out, reducing the overall parallax effect. To test this hypothesis, we analyze an additional dataset in the next section.

Vanishing parallax in multi-cue environments

The sessions analyzed so far restrict the available cues in the environment to a single one. This artificial setting allows us to observe the parallax effect. However, a natural setting will always have an abundance of cues available, which might already mitigate the position-dependent decoding error without the need for active correction.

To test this hypothesis, we analyzed an additional part of the dataset by Duszkiewicz et al. (2024), which consisted of 16 sessions where the animals foraged in a square, open-field environment. Neural activity is again recorded from PoSub (Methods). Again, only a single cue card was positioned on one of the walls, but the environment was square and illuminated, allowing the animals to use additional cues in the environment as anchor (e.g., the corners of the square box).

We found that in these recordings, the parallax effect is drastically reduced compared to the eleven sessions of the previous dataset (weighted mean slope $\overline{w} = -0.04 \pm 0.003$) (Fig. 2c,d,e, green). The distribution of slopes is significantly different from the single-cue dataset (t-test p-value < 0.001, comparing distributions shown in box plots in 2c 'all' condition, Suppl. Tab. 2). Taking only time points into account where the cue card is either directly in front or behind the animal, we see that the effect on the parallax error is less pronounced than in the single cue setting (Fig. 2d, green), observing no significant deviations between the three conditions (t-test p-value > 0.05, Suppl. Tab. 2). Presumably, the abundance of cues at any given time point always mitigates the overall amount of decoding error.

Overall, multiple cues (in combination with AHV integration) appear to eliminate the parallax effect, rendering an additional active position-dependent correction mechanism unnecessary. This might also explain why the parallax effect has not been reported in the literature so far, as most experimental setups allow for multiple cues in the environment to anchor to.

To confirm the hypothesized simple cue-anchoring mechanism, we next sought to model the generation of internal head direction without any active position correction mechanism.

Angular Head Velocity Integration Passively Attenuates Parallax Error

The observation that parallax error exists, but is attenuated through AHV integration and the integration of multiple cues, suggests that the HD system relies on simple visual anchoring without explicit position-dependent correction mechanisms. Previous research has established that HD cells integrate angular head velocity from vestibular and proprioceptive inputs while using visual cues to prevent drift (Blair & Sharp, 1996; McNaughton et al., 1991; Goodridge et al., 1998; Knierim et al., 1995; Zugaro, Berthoz, & Wiener, 2001; Zugaro, Tabuchi, et al., 2001; Bicanski & Burgess, 2016; Ocko et al., 2018; Page & Jeffery, 2018). This integration could naturally attenuate the parallax effect as the visual references are acquired at different positions, thereby averaging out over time. This averaging effect is expected to be much stronger with multiple cues (Gaussier et al., 2019), so complex position-dependent or learning-based correction mechanisms may be unnecessary.

To test this hypothesis quantitatively, we implemented a combined integrate-and-vision model (existing in the literature in various degrees of complexity, e.g., McNaughton et al. (1991, 2006); Page & Jeffery (2018); Bicanski & Burgess (2016)), where the estimated head direction α_{iv} is computed as a weighted sum of the vision-based and AHV-integrated estimates:

$$\alpha_{\text{iv}}(t) = \sigma \cdot \alpha_{\text{int}}(t) + (1-\sigma) \cdot \alpha_{\text{vis}}(t) \cdot v_{cue}(t). \tag{6}$$

σ is a parameter determining the relative weighting of AHV integration and visual anchoring. $v_{cue}(t)$ is a binary variable indicating whether the cue is within the animal's field of vision. The integrated estimate $\alpha_{\text{int}}(t)$ is recursively computed from AHV and the previous state of the integrate-and-vision model:

$$\alpha_{\text{int}}(t) = \alpha_{\text{iv}}(t-1) + \Delta\alpha(t), \tag{7}$$

where $\Delta\alpha(t)$ is the angular displacement derived from head tracking data, assuming noise-free integration (ergo $\text{AHV}(t) = \frac{\Delta\alpha(t)}{\Delta t}$). A sketch of the model is shown in 3a.

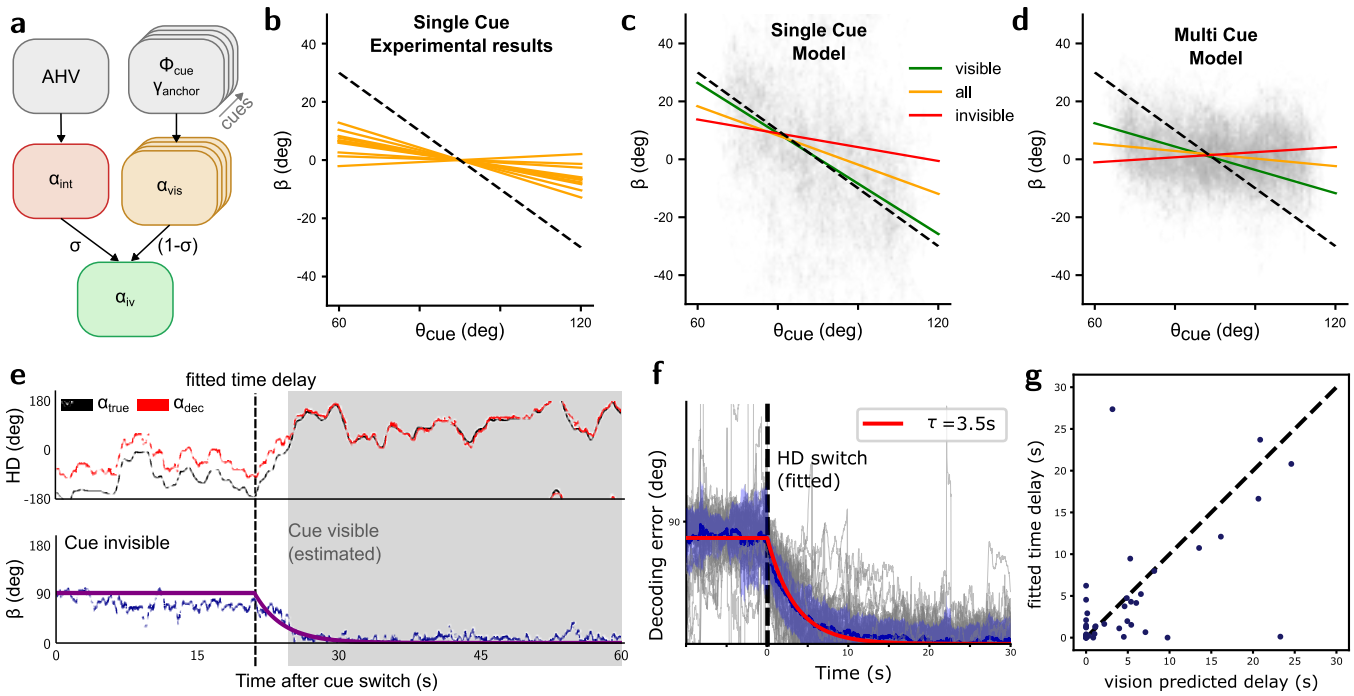

Figure 3: **Simulations confirm that AHV and the use of multiple cues neutralize the measured parallax effect.** (**a**): Visualization of the simulated HD model, as described in Eqs. (6, 7). (**b**): Single-cue experiment experimentally determined linear regression slopes as a reference for the modeling results in panels (c) and (d). (**c**): Fitted slopes from simulated head direction using a single cue. A negative slope with a magnitude below 1 (black dashed line) is observed in all three conditions. The slope is steeper in periods when the cue is visible (green) and less steep when the cue is invisible (red), matching our experimental observations. (**d**): Parallax analysis on the simulated data with multiple cues (cue card and the four corners of the square environment). Overall, parallax is drastically attenuated compared to (b). (**e**): Example beginning of a trial with fitted HD switching onset and exponential decay fit shown in the bottom panel. Grey background color indicates when the cue is visible, according to a 180° field of vision. (**f**): All HD remapping events aligned on the fitted time delay. The resulting mean decay shows a time constant $\tau = 3.5s$, which we use to determine the weighting between visual and integrated HD estimates. (**g**): Distribution of fitted time delays and time delays predicted by a 180° field of vision.

We have two free parameters to define in this model: The weighting σ between the visual-based and the AHV-integrated input, and the field of vision in which a cue is used for anchoring. We set the field of vision to 180° and the weighting parameter $\sigma = 0.997$. The choice of parameters is based on the cue-switching-induced remapping in the single-cue dataset. The viewing angle corresponds to a time delay before the cue switching starts, and the weighting parameter corresponds to the speed at which the switch occurs (Fig. 3d-f, Methods).

In reality, we suspect that the weighting between the AHV integrated and vision-based input is not constant, but dependent on the variance of α_{int} and α_{vis}. Such a dynamic weighting mechanism could explain previously observed phenomena, such as distance-dependent remapping (Zugaro, Berthoz, & Wiener, 2001). However, the variance of α_{int} in the neural system is unknown, and we used the AHV of the tracking system, which is very precise. We therefore fall back on using a fixed weighting σ. To account for the use of the very precise AHV from the tracking system, we additionally add a small amount of random noise on AHV estimate (Gaussian noise, $sd = 0.2\frac{\text{deg}}{\text{timestep}}$).

We repeat the linear regression parallax analysis described above for the modeled HD data, now treating α_{iv} as the internal HD α_{dec}. The modeled HD shows that incorporating AHV integration is sufficient to reduce the parallax error compared to an expected slope of -1 for a solely vision-based model, even in a single cue setting (Fig. 3b, black dashed vs. orange line). Note that the modeled slope w is quite sensitive to the weighting parameter σ, which we cannot estimate reliably. A larger σ results in a lower weighting of the visual anchoring and, consequently, a lower slope. Here, instead of accurately recreating every source of variability, our aim is to show the minimal setup of a model that shows a reduced parallax effect through AHV integration.

The model is also able to capture the difference in slope between cue visibility conditions (Fig. 3b, green and red). Data points where the simulated mouse can see the cue show a higher slope than the ones where the cue is invisible.

Finally, we modeled the effect of multiple cues. For this, we extended the estimation of α_{vis}: We first estimated the

HD signal for each currently visible cue according to Eq. 2 and then calculated the circular mean of these estimates. For simplicity, we assumed an equal weighting between all visible cues. We suppose that in reality this weighting might also be dependent on the variability of each cue's estimate (see Discussion). For additional cues, we choose the four corners of the room. Fig. 3c shows that in such a multi-cue setting, the parallax effect effectively vanishes.

This simplified model of HD formation using AHV signals and egocentric cues demonstrates how the position-dependent parallax effect emerges in a single-cue environment, but is attenuated through AHV integration. Additionally, introducing more cues to the environment practically removes the parallax effect from the resulting HD estimate, making an active correction mechanism superfluous. These model findings are in agreement with the experimental observations of the previous sections.

Inferring the Anchoring Angle from Parallax

So far, we have assumed the anchoring angle to be a fixed angle that defines the mapping between the egocentric 'bearing' angle of a cue and the current head direction. For example, an anchoring angle of 90° might indicate that directly facing the cue corresponds to facing north (head direction north is 90 deg). The anchoring angle γ_{anchor} can be interpreted as the (allocentric) head direction the animal had when it anchored the cue. I.e., the HD system 'decided' that this particular cue has a specific angle offset to its current head direction. This means that at this particular angle, no parallax is expected. In Figs. 2a,b, this corresponds to the x-intercept of the linear regression, which we can compute using the fitted slope and y-intercept:

$$\gamma_{\text{anchor}} = \frac{-b}{w}. \tag{8}$$

Here, we explore whether the anchoring angle of the HD system can be inferred from the spatial distribution of parallax-induced errors. To test this, compute the anchoring angle from the linear fit results as described in Eq. 8 (see Methods for error estimation) and use the obtained γ_{anchor} to compute the expected error β_{vis} in a purely visually guided HD model (Eq. 4). The anchoring angle is very sensitive to slide changes in the obtained slope w. It is therefore not possible with the available data to compute a meaningful anchoring angle for all sessions available. We therefore restrict our further analysis to the seven sessions in the single cue dataset with reliable anchoring angles (standard deviations below 30°). In Fig. 4a, the mean of the observed β_{dec} per position bin is color-coded, showing distinct spatial patterns of systematic error for three example sessions (see Suppl. Fig. 12 for the other 4 sessions). The lower panels in Fig. 4a show theoretical predictions based on the naive anchoring model, demonstrating that the rotation of the anchoring axis qualitatively aligns with the fitted intercept from Fig. 2.

These results indicate that the anchoring angle can be inferred from spatially distributed parallax errors, providing a potential method for calculating it from neural recordings. Furthermore, this analysis supports the notion that HD anchoring occurs at a specific egocentric angle relative to visual landmarks.

Using Eq. 8 to estimate the anchoring angle γ_{anchor}, we can now investigate how stable the anchoring angle, which we have assumed as constant for now, is. To this end, we again split each session into two parts, this time over time into a first half and second half of the recording time (split by the median time point of the included data-points to make both subsets of equal size). Fig. 2b shows that the estimated γ_{anchor} is not significantly different in the first half of the data than in the second half of the data, indicating that the anchoring angle is indeed stable and does not drift significantly over time.

Anchoring angles seem to be distributed around the center (Fig. 2d). A distribution within less than 360° is expected because the HD system can likely only anchor to a cue if it is in the field of vision, and the platform only allows a small movement range. However, at least in this small sample, most anchoring angles are within only about 40°, corresponding to the size of the platform. This could indicate preferred anchoring in an area of increased visual acuity (van Beest et al., 2021) (i.e., when the animal is looking directly at it).

In the single cue dataset, the cue switches positions between trials. We therefore were also interested in whether the anchoring angle is stable between the two cue switches. Out of the seven sessions we included in this sections analysis, we found the decoded HD is consistently remapping with the cue rotation (that is, it shifts by 90° between each trials). Only two sessions (*A3705-200307* and *A3711-200810*) did not show remapping effects. In sessions, where the decoded HD follows these cue switches, the HD system treats the two cues as a single reference, i.e., maintaining the same anchoring angle without re-anchoring. Fig. 2d indeed shows that γ_{anchor} there is no significant change between the two cue conditions, indicating that it remains stable (top five sessions). In sessions that did not show the remapping effect, the error on the anchoring angle increases in the second cue condition, making an assessment of the stability of the stability of the anchoring angle challenging. We speculate, that this effect could be due to the fact that the animal does not treat the rotated cue as the same cue in such cases, and that this increased error could be an effect of the animal using a novel cue to try to anchor to.

These observations and hypotheses should be investigated further in larger environments. Furthermore, to improve the precision of the anchoring angle estimate, it seems necessary to use longer recordings or record more neurons.

What determines the anchoring angle is an interesting question that we can only speculate about here. Presumably, the animal learned a mapping between the cue-specific bearing cell angle representation and the heading direction. We hypothesize that, mechanistically, the anchoring angle may be the angle offset between the cue-specific bearing cell ring(s) and the HD cell ring (Sec. Discussion).

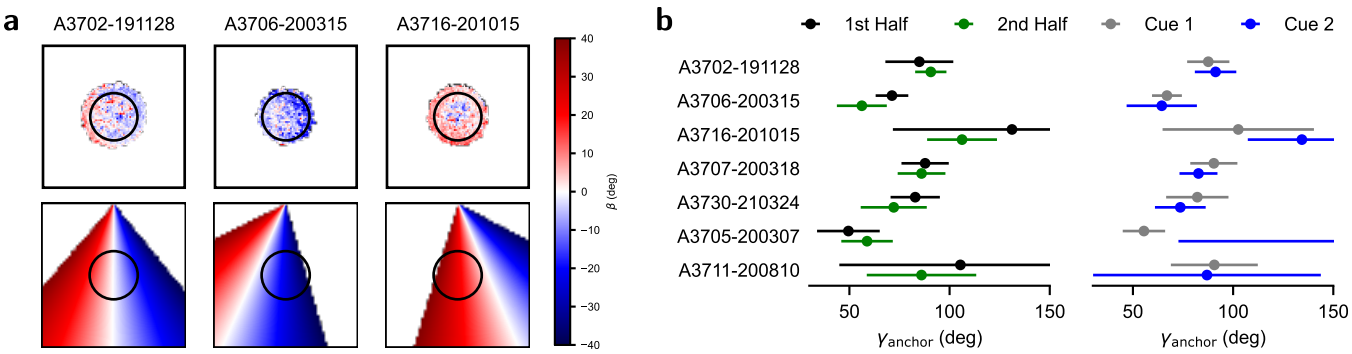

Figure 4: **Estimating the anchoring angle γ_{anchor} based on parallax effects.** (**a**): Top panels: Heat maps of the animal during three different recording sessions, color-coded by the observed angular error β_{dec} of the neural data at each location. Bottom panels: Theoretical predictions of the spatial distribution of β from a purely vision-based HD model. (**b**): Anchoring angles for included sessions from the single-cue dataset, as computed from the linear regression results (Eq. 8). The left panel shows the anchoring angles computed for the first and second halves (split over time) separately. The right panel shows the anchoring angles for the original and rotated cues separately. Both splits indicate that the anchoring angle remains relatively stable over time and across rotations of the cue. Note that the first five sessions in this plots were sessions that exhibited remapping after the cue switch occurred, while the bottom two sessions (*A3705-200307* and *A3711-200810*) did not.

Parallax in individual neuron responses

So far, we focused on analyzing position-dependent errors in the decoded head direction signal, which is a measure based on the population activity of the HD system. To test whether parallax affects the system as a whole or is just a bias introduced by a part of the neurons that are more sensitive to bearing, we also analyze the effect on the single neuron level. Classically, HD neurons are expected to have a single preferred firing direction (PFC) which they are sensitive to. This PFC is estimated from the tuning curve distribution, that is the distribution of true head directions at which the neuron elicits a spike. Assuming a simple cue anchoring model in a single cue environment, we expect the PFC of a neuron to also be position dependent. Under the simple cue anchoring assumption the neuron's PFC would be determined by the egocentric viewing angle of the cue instead of the true current head direction, essentially making the neuron behave similar to a bearing cell.

To test this, we again split each single-cue dataset in two parts, one where the animal is on the right side of the cue, and one where it is on the left. We then compute the tuning curve for each subset of the data (Fig. 5a). To test, whether these two tuning curves (and therefore the neuron's $PFCs$) are systematically shifted against one another, we compute the cross-correlation between the left and right tuning curve and determine the peak of the cross-correlation as the amount of PFC-shift. As shown in Fig. 5b, we indeed see a bias towards a negative shift, as expected. Statistical analysis reveals that the single-cue dataset shows a highly significant leftward shift (mean = $-3.86^\circ \pm 0.88^\circ$, $n = 823$ neurons, $p = 1.35 \times 10^{-5}$, one-sample t-test).

In the multi-cue data, the effect is weaker but still significant (mean = $-1.16^\circ \pm 0.45^\circ$, $n = 1041$ neurons, $p = 0.011$, one-sample t-test). The shift magnitude differs significantly between conditions ($p = 6.55 \times 10^{-3}$, two-sample t-test), confirming the result of the system-level analysis, that multiple cues help correct for the parallax error from each individual cue.

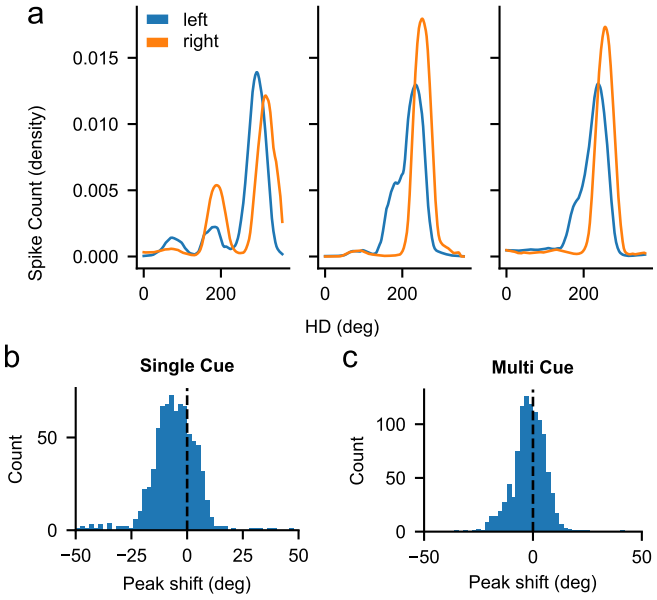

Figure 5: **Single neuron analysis results**. **(a)**: Three examples of neural tuning curves for the subset of recording data where the animal is on the left (blue) and right (orange) side of the cue. **(b,c)**: Histogram of the peaks found in the cross-correlations between the left and right tuning curves. **(b)** shows results for the neurons in the single-cue datasets, **(c)** shows the results for the multi-cue dataset. (b) and (c) show neurons of all recording sessions ($N_b = 11$, $N_c = 16$).

A model for HD formation

The findings presented in this work suggest a specific model of how visual input is integrated in the HD network. A major challenge of this integration is the fact, that visual observations are inherently egocentric, but the head direction is an allocentric signal. Therefore, the HD network needs to perform an egocentric-to-allocentric coordinate transform. This coordinate transform is widely believed to happen in the retrosplenial cortex (RSC) and the mapping between RSC and the postsubiculum (PoSub). Bearing cells, which encode the egocentric angle to specific objects, have largely been found in RSC. PoSub receives input both from the visual HD pathway through the RSC, as well as from the movement integrating pathway through the antero-dorsal nucleus (AdN). For a detailed description of the movement integration pathway and how to model it, see Bicanski & Burgess (2016).

An open question in the literature so far is the exact mechanism that allows the egocentric-to-allocentric transformation in the HD network. Given the experimental results provided in this study, we propose the following solution: Bearing cells in RSC map onto a HD ring attractor in PoSub with a fixed offset. This fixed offset is what determines the anchoring angle in the previous analysis. Specific bearing cell ring attractors may be activated by visual cues, whose identity and egocentric position is provided by the visual system.

Any single bearing cell ring attractor is subject to the parallax effect. Therefore, in a highly restricted setting of only one singular cue in the environment, this parallax error is also present in the postsubiculum. However, in practice we always observe multiple bearing cell ring attractors being active for multiple cues. The postsubiculum at this point acts as the average approximation of all visual estimates together with the movement integrated input from the AdN (akin to the simulated α_{iv} in the previous section).

The weighting between the different bearing cell rings and the AdN input could be established by the gain of each population (effectively the 'height of the activity bump in each ring attractor'). We speculate that the gain of each ring attractor is determined by how fast the activity bump is moving along the attractor manifold, where immobile activity bumps are weighted higher than fast moving ones. Such a weighting mechanism would result in close-by visual cues to influence the PoSub HD less, as their egocentric bearing changes faster than those of more distant cues. This weighting would also give more weight to stationary objects rather than moving ones. It would finally also weigh movement integrated estimates vs. visual estimates, relying stronger on vision when the head is moved quickly and the movement integration is more prone to inaccurate HD estimates.

Finally, as already suggested in previous studies, we suspect PoSub sends its combined HD signal back to RSC and AdN as a correction mechanism. Additionally we expect the PoSub to propagate the combined HD estimate forward to the hippocampal formation for subsequent position estimation.

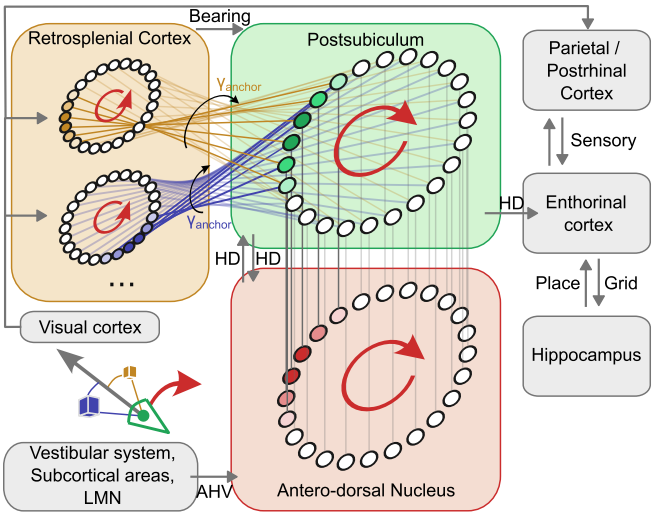

Figure 6: **Conceptual model of the HD formation from combined AHV integration and visual inputs**. Based on visual inputs and inertial movement measurements (bottom left), visual cortices and subcortical areas transmit information along different pathways. The visual information is mapped to bearing cell rings in retrosplenial cortex (RSC). These in turn have a fixed anchoring angle to map onto the head direction cells in the postsubiculum (PoSub). The inertial measurements in turn are projected through LMN to the Antero-dorsal Nucleus (AdN) (see Bicanski & Burgess (2016) for a detailed description of this mechanism). PoSub acts as a central integrator in this model, combining the visiual and integrated HD states and relaying them back to RSC and AdN and projecting them forward to the entorhinal cortex for subsequent position-estimation in the hippocampal formation.

Discussion

Spatial navigation requires a stable allocentric sense of direction, yet sensory cues are perceived egocentrically. This necessitates a coordinate transformation whose underlying neural mechanism has been a long-standing question (J. S. Taube, 2007; Zhang, 1996). In this study, we provide evidence for a systematic parallax error in the head-direction (HD) signal of mice navigating an environment with only a single visual cue. This finding indicates that the HD system does not employ a complex, position-dependent correction mechanism, for instance through place cell feedback, which would introduce a circular dependency, as place cells themselves require a stable HD signal (Bicanski & Burgess, 2016; McNaughton et al., 2006). Instead, our results support a model where the system relies on a simple, computationally efficient egocentric cue-anchoring strategy for the ego-to-allocentric transformation (Skaggs et al., 1994; Page & Jeffery, 2018). This process, while effective, inherently introduces a predictable, position-dependent bias when referencing a single, nearby landmark.

The artificial nature of a single-cue environment provides a unique window into the mechanism of this transformation.

Understanding this mechanism is critical, as a stable allocentric HD signal is a fundamental prerequisite for downstream circuits in the hippocampal formation to build and maintain a coherent cognitive map (McNaughton et al., 2006; Tan et al., 2017). Our findings are consistent with a model where bearing cells in the retrosplenial cortex (RSC), which encode the egocentric angle to specific cues, map onto the HD ring attractor in the postsubiculum (PoSub) with a fixed angular offset (Alexander et al., 2020; Bicanski & Burgess, 2020). We term this offset the anchoring angle (γ_{anchor}), which defines the relationship between the sensory input and the animal's internal sense of direction. A key contribution of our work is demonstrating that the properties of this anchoring angle can be elucidated from the spatial pattern of parallax errors, and that it remains relatively stable throughout a session. This direct mapping strategy is fast and computationally efficient, as it does not require explicit positional information to compute an HD estimate. Such efficiency is a critical advantage for both biological and artificial navigation systems where energy and processing resources are constrained (Renner et al., 2022; Arleo & Gerstner, 2000). This work highlights a fundamental trade-off between computational simplicity and absolute positional accuracy in neural coding.

The absence of previous reports on this parallax effect warrants explanation. Our findings suggest two primary reasons. First, the HD system continuously integrates angular head velocity (AHV), which inherently smooths and reduces the visual error over time as the animal moves through the environment (McNaughton et al., 1991; J. S. Taube, 2007). Our data directly support this, showing that the measured parallax error was significantly attenuated when the cue was not in the animal's direct field of view. Second, and more importantly, naturalistic environments are rich with visual and and other directional sensory cues. Our analysis of recordings from a multi-cue setting revealed a drastic reduction and practical elimination of the parallax error. This strongly supports the hypothesis that the HD system averages heading estimates derived from multiple landmarks to form a unified, robust signal (Gaussier et al., 2019; Goodridge et al., 1998). The individual parallax errors associated with each cue, having different spatial dependencies, effectively cancel each other out. Most experimental paradigms, even those with a primary cue card, likely provide sufficient secondary cues (e.g., arena corners, shadows, equipment, odors, sounds) to enable this averaging, thus masking the parallax from any single cue.

The impact of parallax is not limited to a subset of specialized cells but is a system-wide phenomenon. Our single-neuron analysis revealed that the preferred firing directions (PFDs) of individual HD neurons shift systematically with the animal's position relative to the cue. This confirms that the entire HD attractor network is biased by the visual input in the single-cue context, rather than the effect being an artifact of a few bearing-like cells.

While this study provides strong support for a simple anchoring model, certain limitations should be acknowledged. Our conclusions are drawn from a single dataset, and validation in other contexts is necessary. The simplified integrate-and-vision model we presented was intended to demonstrate the principle of passive parallax attenuation, not to capture the full complexity of multisensory integration, which likely involves dynamic weighting based on cue stability, distance, and familiarity (Cheng et al., 2007; Julian et al., 2018). The specific nature of the cue, here a bright, unreachable LED, may have influenced how it was perceived, perhaps as a more distal (celestial) cue than its physical location would suggest (Giraldo et al., 2018).

Future research should build on these findings to further probe the mechanics of cue integration. A crucial experiment would be to use a controlled environment with two distinct cues at different angular separations to explicitly test our model's prediction that the resulting HD signal reflects a weighted average of the two independent parallax effects (Suppl. Sec. Modeling the parallax error with two cues). Systematically manipulating cue distance and salience would also allow for an investigation into how the system weights proximal versus distal landmarks, potentially revealing dynamic gain-control mechanisms where more stable, distant cues are given greater influence (Zugaro, Berthoz, & Wiener, 2001; Blair & Sharp, 1996). Finally, investigating whether parallax error propagates to other nodes of the navigation circuit, such as the LMN or entorhinal cortex, could further elucidate how the brain ensures a stable directional reference for navigation.

In conclusion, our study demonstrates that the mammalian HD system is subject to parallax error when constrained to a single visual landmark. This finding strongly supports a model of simple egocentric cue-anchoring, a computationally efficient strategy for ego-to-allocentric transformation. The apparent vulnerability to error is robustly overcome in natural settings through the parallel integration of self-motion cues and the averaging of information from multiple environmental landmarks. This work clarifies a key mechanism of spatial cognition and highlights an elegant solution for generating a stable allocentric signal, offering insights that can inform the development of more robust and efficient bio-inspired navigation systems.

Methods

Single Cue experiment

We analyzed publicly available neural recordings from the postsubiculum (PoSub) of six mice during the "Cue Rotation Task" reported in (Duszkiewicz et al., 2024). We were additionally provided with 5 previously unpublished sessions of the same experimental setup, so overall we are able to report on 11 datasets. Each dataset includes tracked head position and direction and spike trains. Mice freely explored a 30 cm diameter elevated circular arena within a 90 cm darkened square enclosure (Fig. 1A) for approximately 75 minutes per session. Visual cues, consisting of dim LED strips forming a "V" or "X" shape (approximately 10 cm wide), were positioned at the center of each wall and treated as point sources for

analysis. Surgical procedures, electrophysiological recording details, and the exact experimental protocol are described in (Duszkiewicz et al., 2024). Each session began with a stable cue presentation (15-20 minutes). Subsequently, this initial cue was turned off, and a cue on an adjacent wall was activated. Only one cue was active at any time. The experimental protocol comprised 16 200-second trials, with the active cue alternating between the two LEDs after each trial. In the additionally provided 5 datasets, the mice's HD neurons did not remap during the cue rotation, but kept their orientation throughout the sessions.

Multi Cue experiment

We also analyzed publicly available square open field recordings of 16 mice from the same publication (Duszkiewicz et al., 2024). Neural activity was again recorded from PoSub and the animals position and head direction were tracked. The environment consisted of a 90 cm x 90 cm square box with a single cue card on one of the walls to serve as a cue. Surgical procedures, electrophysiological recording details, and the exact experimental protocol are again described in (Duszkiewicz et al., 2024).

Data Exclusion

In all datasets we excluded periods where the mice exhibited prolonged immobility, as these periods led to fewer activity and an unreliable decoded HD signal. We achieved this, by estimating the animals speed from the tracked position. We then smoothed this position signal (square kernel, 0.5 s width) and rejected time periods in which the absolute value of the smoothed speed was below $2\frac{cm}{s}$. We additionally excluded the time periods that were used to compute the tuning curves for each neuron from all further analysis. For the tuning curve estimation, we used the first 10 min of each recording.

In the single cue experiment sessions, we also estimated the time period of HD remapping in the beginning of the trial and excluded these time windows from the parallax analysis. In the sessions without remapping, we only considered the trials of the original cue orientation.

HD Decoding

As Duszkiewicz et al. (2024), we performed Bayesian decoding (Zhang et al., 1998) on the head direction cells (cell labeling adopted from the dataset). Tuning curves for all head direction neurons were computed using the first 10 minutes of the recording (part of the habituation period in the single cue experiment and just the first 10 min of recording in the square arena dataset). This period was excluded from subsequent analysis. The Bayesian decoder treats these tuning curves as conditional probability distributions of head direction given a neuron's firing. For each time bin of 10 ms, the likelihood distribution of the head direction was calculated by multiplying the tuning curves of all spiking neurons within that bin. The prior is the head direction distribution of the preceding time bin and discourages large jumps between consecutive estimates. The head direction estimate for each time bin was then obtained by identifying the peak of the resulting posterior. Notably, the number of HD neurons per dataset varied between all sessions ($25-117$ recorded HD units, mean: 69 ± 23 units). This led to a difference in decoding quality ($RMSE: 0.75^\circ - 1.6^\circ$, mean RMSE: $1.1^\circ \pm 0.2^\circ$). RMSE and number of neurons for all sessions can be found in Suppl. Fig. 14.

Linear regression and bootstrapping

We use a linear regression between the decoding error β and the allocentric cue angle θ_{cue} to measure the amount of parallax and determine the anchoring angle. The linear regression is implemented as a least square optimizer using the "SciPy" package in python. To account for autocorrelations in the time series data, we use stationary block bootstrapping (Politis & and, 1994) with an average block length of 2.5 s and n=1000 iterations to estimate the slopes, intercepts and standard errors of w and b, as well as the p-values for the respective fits.

Computing the anchoring angle

The anchoring angle γ_{anchor} is calculated from the results of the bootstrapped linear regression as $\gamma_{\text{anchor}} = -b/w$ (Eq. 8). Uncertainties were propagated using standard error propagation:

$$\sigma_\gamma = |\gamma_{\text{anchor}}| \times \sqrt{\left(\frac{\sigma_b}{b}\right)^2 + \left(\frac{\sigma_w}{w}\right)^2}, \tag{9}$$

where σ_b and σ_w are the bootstrapped standard errors of the intercept and slope, respectively.

Determining field of vision and weighting from cue switches

The integrate-and-vision model (Eq. 6) is dependent on a weighting factor σ and the field of vision. Both parameters can be estimated by analyzing the cue-switching periods of the single cue experiment recordings. In the beginning of each trial of these sessions, we see a remapping event, where the decoded HD takes some time to adjust to the new cues position. We estimate this period by fitting a delayed exponential decay to the decoding error in these periods (Fig. 3d, purple). The time constant of the exponential decay τ tells us how fast the visual input changes the current HD estimate and is directly related to the weighting of the integrated and the visual input by $\sigma = e^{-\frac{1}{tau \cdot s}}$, where s is the sampling rate. As we find the mean time constant is $\tau = 3.5\ s$ (Fig. 3e), we obtain a weighting factor $\sigma = 0.997$.

Furthermore, we hypothesize that the delay before the onset of the exponential decay might be due to the effective field of vision of the animal, that is the viewing angle range in which the animals are using landmarks for the visual anchoring. Based on the fitted anchoring angle, we observe that an effective field of vision of 180° best fits the fitted time delays (Fig. 3d,f).

Software

Code was written in Python 3.12 using numpy, matplotlib, and scipy for analysis and visualization. Fits were performed using the scipy.stats.linregress function, bootstrapping using the

arch package and MSE minimization for σ using the optuna package.

Acknowledgements

For this work, the data from Duszkiewicz et al. (2024) was used, and we thank the authors for making this data available. The data can be found here: 10.6084/m9.figshare.24921252. We thank Johannes Leugering and Paxon Frady for their feedback. Generative AI was used to optimize and document code and to support writing. This research is funded by VolkswagenStiftung [CLAM 9C854].

References

Alexander, A. S., Carstensen, L. C., Hinman, J. R., Raudies, F., Chapman, G. W., & Hasselmo, M. E. (2020). Egocentric boundary vector tuning of the retrosplenial cortex. *Science advances*, *6*(8), eaaz2322.

Arleo, A., & Gerstner, W. (2000). Modeling rodent head-direction cells and place cells for spatial learning in biomimetic robotics. *From Animals to Animats*, *6*, 236–245.

Bicanski, A., & Burgess, N. (2016). Environmental anchoring of head direction in a computational model of retrosplenial cortex. *Journal of Neuroscience*, *36*(46), 11601–11618.

Bicanski, A., & Burgess, N. (2020, September). Neuronal vector coding in spatial cognition. *Nature Reviews Neuroscience*, *21*(9), 453–470. doi: 10.1038/s41583-020-0336-9

Blair, H. T., & Sharp, P. E. (1996). Visual and vestibular influences on head-direction cells in the anterior thalamus of the rat. *Behavioral neuroscience*, *110*(4), 643.

Boucheny, C., Brunel, N., & Arleo, A. (2005, March). A Continuous Attractor Network Model Without Recurrent Excitation: Maintenance and Integration in the Head Direction Cell System. *Journal of Computational Neuroscience*, *18*(2), 205–227. doi: 10.1007/s10827-005-6559-y

Burak, Y., & Fiete, I. R. (2009, February). Accurate Path Integration in Continuous Attractor Network Models of Grid Cells. *PLoS Computational Biology*, *5*(2), e1000291. doi: 10.1371/journal.pcbi.1000291

Chaudhuri, R., Gerçek, B., Pandey, B., Peyrache, A., & Fiete, I. (2019, September). The intrinsic attractor manifold and population dynamics of a canonical cognitive circuit across waking and sleep. *Nature Neuroscience*, *22*(9), 1512–1520. doi: 10.1038/s41593-019-0460-x

Cheng, K., Shettleworth, S. J., Huttenlocher, J., & Rieser, J. J. (2007). Bayesian integration of spatial information. *Psychological bulletin*, *133*(4), 625.

Duszkiewicz, A. J., Orhan, P., Skromne Carrasco, S., Brown, E. H., Owczarek, E., Vite, G. R., ... Peyrache, A. (2024, April). Local origin of excitatory–inhibitory tuning equivalence in a cortical network. *Nature Neuroscience*, *27*(4), 782–792. doi: 10.1038/s41593-024-01588-5

Gaussier, P., Banquet, J. P., Cuperlier, N., Quoy, M., Aubin, L., Jacob, P.-Y., ... Poucet, B. (2019). Merging information in the entorhinal cortex: what can we learn from robotics experiments and modeling? *Journal of Experimental Biology*, *222*(Suppl_1), jeb186932.

Giocomo, L. M., Stensola, T., Bonnevie, T., Van Cauter, T., Moser, M.-B., & Moser, E. I. (2014). Topography of head direction cells in medial entorhinal cortex. *Current Biology*, *24*(3), 252–262.

Giraldo, Y. M., Leitch, K. J., Ros, I. G., Warren, T. L., Weir, P. T., & Dickinson, M. H. (2018). Sun navigation requires compass neurons in drosophila. *Current Biology*, *28*(17), 2845–2852.

Golob, E. J., & Taube, J. S. (1997, July). Head direction cells and episodic spatial information in rats without a hippocampus. *Proceedings of the National Academy of Sciences*, *94*(14), 7645–7650. doi: 10.1073/pnas.94.14.7645

Goodridge, J. P., Dudchenko, P. A., Worboys, K. A., Golob, E. J., & Taube, J. S. (1998). Cue control and head direction cells. *Behavioral neuroscience*, *112*(4), 749.

Hahnloser, R. H. R. (2003, September). Emergence of neural integration in the head-direction system by visual supervision. *Neuroscience*, *120*(3), 877–891. doi: 10.1016/S0306-4522(03)00201-X

Hulse, B. K., & Jayaraman, V. (2020). Mechanisms underlying the neural computation of head direction. *Annual review of neuroscience*, *43*(1), 31–54.

Julian, J. B., Keinath, A. T., Marchette, S. A., & Epstein, R. A. (2018). The neurocognitive basis of spatial reorientation. *Current Biology*, *28*(17), R1059–R1073.

Knierim, J. J., Kudrimoti, H. S., & McNaughton, B. L. (1995). Place cells, head direction cells, and the learning of landmark stability. *Journal of Neuroscience*, *15*(3), 1648–1659.

McNaughton, B. L., Battaglia, F. P., Jensen, O., Moser, E. I., & Moser, M.-B. (2006, August). Path integration and the neural basis of the 'cognitive map'. *Nature Reviews Neuroscience*, *7*(8), 663–678. doi: 10.1038/nrn1932

McNaughton, B. L., Chen, L., & Markus, E. (1991). "dead reckoning," landmark learning, and the sense of direction: a neurophysiological and computational hypothesis. *Journal of Cognitive Neuroscience*, *3*(2), 190–202.

Mizumori, S., & Williams, J. (1993, September). Directionally selective mnemonic properties of neurons in the lateral dorsal nucleus of the thalamus of rats. *The Journal of Neuroscience*, *13*(9), 4015–4028. doi: 10.1523/JNEUROSCI.13-09-04015.1993

Ocko, S. A., Hardcastle, K., Giocomo, L. M., & Ganguli, S. (2018). Emergent elasticity in the neural code for space. *Proceedings of the National Academy of Sciences*, *115*(50), E11798–E11806.

Page, H. J., & Jeffery, K. J. (2018). Landmark-based updating of the head direction system by retrosplenial cortex: a computational model. *Frontiers in Cellular Neuroscience*, *12*, 191.

Politis, D. N., & and, J. P. R. (1994). The stationary bootstrap. *Journal of the American Statistical Association*, *89*(428), 1303–1313. Retrieved from https://doi.org/10.1080/01621459.1994.10476870 doi: 10.1080/01621459.1994.10476870

Rank, J. (1984). Head-direction cells in the deep layers of dorsal presubiculum of freely moving rats. In *Soc. neuroscience abstr.* (Vol. 10, p. 599).

Redish, A. D., Elga, A. N., & Touretzky, D. S. (1996). A coupled attractor model of the rodent head direction system. *Network: computation in neural systems*, *7*(4), 671.

Renner, A., Supic, L., Danielescu, A., Indiveri, G., Frady, E. P., Sommer, F. T., & Sandamirskaya, Y. (2022). Visual odometry with neuromorphic resonator networks. *arXiv preprint arXiv:2209.02000*.

Skaggs, W., Knierim, J., Kudrimoti, H., & McNaughton, B. (1994). A model of the neural basis of the rat's sense of direction. *Advances in neural information processing systems*, *7*.

Stackman, R. W., & Taube, J. S. (1998). Firing properties of rat lateral mammillary single units: head direction, head pitch, and angular head velocity. *Journal of Neuroscience*, *18*(21), 9020–9037.

Tan, H. M., Wills, T. J., & Cacucci, F. (2017). The development of spatial and memory circuits in the rat. *WIREs Cognitive Science*, *8*(3), e1424. doi: 10.1002/wcs.1424

Taube, J., Muller, R., & Ranck, J. (1990, February). Head-direction cells recorded from the postsubiculum in freely moving rats. II. Effects of environmental manipulations. *The Journal of Neuroscience*, *10*(2), 436–447. doi: 10.1523/JNEUROSCI.10-02-00436.1990

Taube, J. S. (1995). Head direction cells recorded in the anterior thalamic nuclei of freely moving rats. *Journal of Neuroscience*, *15*(1), 70–86.

Taube, J. S. (2007, July). The Head Direction Signal: Origins and Sensory-Motor Integration. *Annual Review of Neuroscience*, *30*(Volume 30, 2007), 181–207. doi: 10.1146/annurev.neuro.29.051605.112854

Taube, J. S., Muller, R. U., & Ranck, J. B. (1990). Head-direction cells recorded from the postsubiculum in freely moving rats. ii. effects of environmental manipulations. *Journal of Neuroscience*, *10*(2), 436–447.

van Beest, E. H., Mukherjee, S., Kirchberger, L., Schnabel, U. H., van der Togt, C., Teeuwen, R. R., ... others (2021). Mouse visual cortex contains a region of enhanced spatial resolution. *Nature communications*, *12*(1), 4029.

Zhang, K. (1996). Representation of spatial orientation by the intrinsic dynamics of the head-direction cell ensemble: a theory. *Journal of Neuroscience*, *16*(6), 2112–2126.

Zhang, K., Ginzburg, I., McNaughton, B. L., & Sejnowski, T. J. (1998). Interpreting neuronal population activity by reconstruction: unified framework with application to hippocampal place cells. *Journal of neurophysiology*, *79*(2), 1017–1044.

Zugaro, M. B., Arleo, A., Berthoz, A., & Wiener, S. I. (2003, April). Rapid Spatial Reorientation and Head Direction Cells. *Journal of Neuroscience*, *23*(8), 3478–3482. doi: 10.1523/JNEUROSCI.23-08-03478.2003

Zugaro, M. B., Berthoz, A., & Wiener, S. I. (2001, July). Background, But Not Foreground, Spatial Cues Are Taken as References for Head Direction Responses by Rat Anterodorsal Thalamus Neurons. *The Journal of Neuroscience*, *21*(14), RC154-RC154. doi: 10.1523/JNEUROSCI.21-14-j0001.2001

Zugaro, M. B., Tabuchi, E., Fouquier, C., Berthoz, A., & Wiener, S. I. (2001). Active locomotion increases peak firing rates of anterodorsal thalamic head direction cells. *Journal of neurophysiology*, *86*(2), 692–702.

Supplementary Material

Modeling the parallax error with two cues

As explained in the discussion, one promising future direction of research to test the simple cue-anchoring hypothesis is the study of restricted experimental environments with sparse cues. Previously, we discussed two experimental setups and their effects in the model - (1) A single cue leads to a linear relationship between decoding error and allocentric cue angle, and (2) An abundance of cue decreases this slope close to zero, effectively making the parallax effect undetectable.

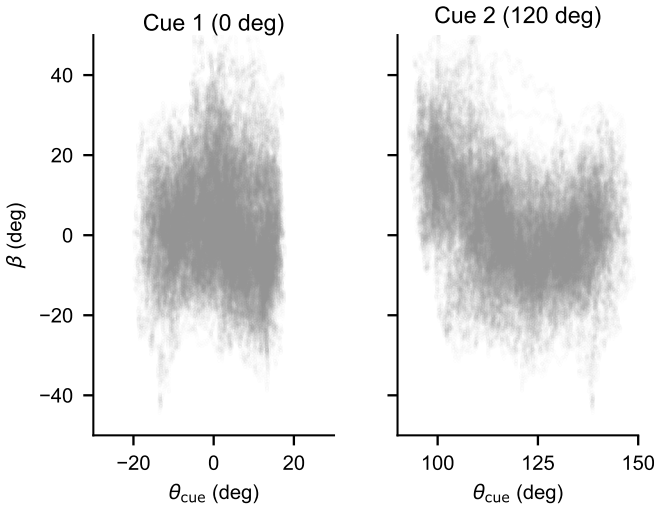

Figure 7: **Modeled parallax effect in an environment with two cues.** The two cues are position 120° apart and at equal distance. The two panels show the decoding error β plotting against each of the two allocentric cue angles θ_{cue}.

We additionally modeled a third case, where there are only two cues available to the integrate-and-vision model. These sparse available cue lead to a non-linear relationship between the decoding error β and the allocentric cue angle θ_{cue}.

Significance testing results

Table 1: Statistical comparison of decoding errors between left and right arena positions across all recording sessions in the single cue dataset. All p-values remain significant after Bonferroni correction for multiple comparisons ($\alpha = 0.0045$). Effect sizes: negligible ($|d| < 0.2$), small ($0.2 \leq |d| < 0.5$), medium ($0.5 \leq |d| < 0.8$), large ($|d| \geq 0.8$).

Session	Sample Size		Left Side		Right Side		Test	Statistics			Effect	Effect
	Left	Right	Mean (°)	SD (°)	Mean (°)	SD (°)	Type	t-stat	df	p-value	Cohen's d	Size
A3702-191128	69,417	74,450	3.011	14.640	-4.783	12.561	Welch's	108.00	137159.5	< 0.001	0.57	Medium
A3706-200315	43,598	24,753	-3.988	10.257	-16.873	12.570	Welch's	137.39	43476.6	< 0.001	1.16	Large
A3716-201015	54,813	57,448	4.295	17.628	2.250	14.995	Welch's	20.89	107660.9	< 0.001	0.13	Negligible
A3707-200318	82,481	57,669	4.122	13.801	-3.105	12.571	Welch's	101.70	130845.0	< 0.001	0.54	Medium
A3717-201022	17,240	81,368	1.737	19.206	-2.230	20.188	Welch's	24.41	25953.3	< 0.001	0.20	Negligible
A3730-210324	38,263	35,356	0.457	10.843	-3.095	10.164	Welch's	45.88	73601.8	< 0.001	0.34	Small
A3701-191120	58,524	135,020	2.005	16.143	-0.211	12.299	Welch's	29.68	89228.8	< 0.001	0.16	Negligible
A3705-200307	52,669	60,660	-4.433	12.816	-10.625	13.461	Student's	78.97	113327.0	< 0.001	0.47	Small
A3711-200815	23,141	15,398	3.871	22.702	-5.200	28.219	Student's	34.81	38537.0	< 0.001	0.36	Small
A3711-200810	37,485	45,425	2.351	15.850	-2.117	14.414	Welch's	42.08	76647.8	< 0.001	0.30	Small
A3712-200903b	68,480	35,945	-8.725	17.593	-6.250	14.205	Welch's	-24.58	87385.6	< 0.001	-0.15	Negligible

* Test type determined by Levene's test for equality of variances

Table 2: Statistical comparison of slope distributions across viewing conditions and datasets. Slopes represent the relationship between landmark angle and decoding error. Significance levels: *** $p < 0.001$, ** $p < 0.01$, * $p < 0.05$, ns = not significant.

Dataset	Condition 1	Condition 2	Test	p-value	Significance
Single Cue					
	Visible	Invisible	t-test	< 0.001	***
	All	Invisible	t-test	0.010	*
	Visible	All	t-test	0.001	**
Multi Cue					
	Visible	Invisible	t-test	0.169	ns
	All	Invisible	t-test	0.497	ns
	Visible	All	t-test	0.327	ns
Between Datasets					
	Single Cue Invisible	Multi Cue Invisible	t-test	0.827	ns
	Single Cue All	Multi Cue All	t-test	< 0.001	***
	Single Cue Visible	Multi Cue Visible	t-test	< 0.001	***

All comparisons used independent samples t-tests after Shapiro-Wilk normality testing

Table 3: Parallax Analysis Results - Single Cue. Anchoring angles with errors $> 180°$ are not reported.

Session	Condition	w	SD	p-value	R^2	γ_{anchor} (deg)	Significance
A3702-191128	Invisible	-0.030	0.030	0.309	0.001	-56.5 ± 105.9	ns
	All data	-0.346	0.020	< 0.001	0.084	89.3 ± 7.5	***
	Visible	-0.888	0.061	< 0.001	0.279	95.8 ± 9.3	***
A3706-200315	Invisible	-0.233	0.067	< 0.001	0.026	60.2 ± 28.4	***
	All data	-0.428	0.029	< 0.001	0.127	66.3 ± 7.3	***
	Visible	-0.758	0.089	< 0.001	0.174	79.0 ± 14.8	***
A3716-201015	Invisible	0.091	0.066	0.167	0.001	4.7 ± 64.7	ns
	All data	-0.197	0.025	< 0.001	0.009	112.7 ± 18.5	***
	Visible	-0.467	0.052	< 0.001	0.078	96.2 ± 15.0	***
A3707-200318	Invisible	-0.308	0.048	< 0.001	0.069	81.2 ± 20.4	***
	All data	-0.275	0.018	< 0.001	0.072	87.1 ± 8.3	***
	Visible	-0.127	0.078	0.103	0.008	90.5 ± 71.9	ns
A3717-201022	Invisible	-0.006	0.085	0.944	0.000	-	ns
	All data	-0.087	0.044	0.045	0.001	66.3 ± 59.0	*
	Visible	-0.438	0.080	< 0.001	0.042	93.1 ± 25.0	***
A3730-210324	Invisible	-0.106	0.041	0.010	0.004	47.0 ± 40.8	**
	All data	-0.222	0.019	< 0.001	0.032	78.1 ± 10.2	***
	Visible	-0.297	0.055	< 0.001	0.042	83.3 ± 22.4	***
A3701-191120	Invisible	0.248	0.046	< 0.001	0.035	82.6 ± 23.8	***
	All data	-0.044	0.021	0.038	0.002	91.0 ± 64.5	*
	Visible	-0.330	0.038	< 0.001	0.110	72.8 ± 13.5	***
A3705-200307	Invisible	0.054	0.047	0.256	0.002	-	ns
	All data	-0.255	0.025	< 0.001	0.044	55.3 ± 10.3	***
	Visible	-0.516	0.080	< 0.001	0.121	75.1 ± 19.4	***
A3711-200815	Invisible	-0.009	0.186	0.963	0.000	-	ns
	All data	-0.227	0.084	0.007	0.005	74.0 ± 43.6	**
	Visible	-0.616	0.197	0.002	0.038	83.1 ± 38.2	**
A3711-200810	Invisible	-0.045	0.050	0.368	0.001	30.7 ± 106.1	ns
	All data	-0.214	0.036	< 0.001	0.017	90.8 ± 21.9	***
	Visible	-0.495	0.152	0.001	0.041	103.7 ± 43.0	**
A3712-200903b	Invisible	0.381	0.074	< 0.001	0.036	109.6 ± 27.8	***
	All data	0.069	0.040	0.082	0.001	196.5 ± 123.7	ns
	Visible	-0.620	0.089	< 0.001	0.055	76.8 ± 16.8	***

Table 4: Parallax Analysis Results - Multi Cue. Anchoring angles with errors $> 180^\circ$ are not reported.

Session	Condition	w	SD	p-value	R^2	γ_{anchor} (deg)	Significance
A3701	Invisible	-0.089	0.017	< 0.001	0.044	50.1 ± 20.6	***
	All data	-0.032	0.010	0.002	0.006	59.4 ± 36.7	**
	Visible	0.129	0.026	< 0.001	0.063	83.9 ± 27.7	***
A3702	Invisible	-0.012	0.012	0.329	0.001	-	ns
	All data	-0.040	0.011	< 0.001	0.010	4.9 ± 24.3	***
	Visible	-0.044	0.024	0.067	0.012	94.8 ± 68.8	ns
A3703	Invisible	-0.033	0.010	0.001	0.013	96.7 ± 40.4	**
	All data	-0.016	0.008	0.050	0.002	88.3 ± 61.4	*
	Visible	0.001	0.028	0.983	0.000	-	ns
A3705	Invisible	0.060	0.024	0.011	0.015	136.7 ± 67.4	*
	All data	-0.031	0.012	0.009	0.005	-13.7 ± 38.7	**
	Visible	-0.194	0.019	< 0.001	0.210	76.4 ± 11.5	***
A3706	Invisible	-0.069	0.024	0.004	0.028	-38.6 ± 27.1	**
	All data	-0.072	0.010	< 0.001	0.035	-22.7 ± 13.0	***
	Visible	-0.138	0.016	< 0.001	0.111	42.6 ± 12.5	***
A3707	Invisible	-0.061	0.029	0.032	0.015	-5.1 ± 60.3	*
	All data	-0.077	0.014	< 0.001	0.051	36.6 ± 20.1	***
	Visible	-0.224	0.034	< 0.001	0.289	61.7 ± 16.0	***
A3708	Invisible	0.134	0.027	< 0.001	0.096	71.6 ± 24.0	***
	All data	0.090	0.019	< 0.001	0.027	67.9 ± 24.4	***
	Visible	-0.213	0.067	0.001	0.044	105.0 ± 44.9	**
A3710	Invisible	0.009	0.024	0.699	0.000	-	ns
	All data	-0.000	0.014	0.983	0.000	-	ns
	Visible	-0.060	0.019	0.002	0.013	67.5 ± 36.7	**
A3711	Invisible	0.031	0.026	0.231	0.003	115.2 ± 127.1	ns
	All data	0.034	0.020	0.093	0.003	64.2 ± 64.3	ns
	Visible	0.074	0.039	0.056	0.012	48.9 ± 54.6	ns
A3712	Invisible	0.078	0.041	0.061	0.008	183.8 ± 108.3	ns
	All data	-0.050	0.020	0.013	0.002	-10.7 ± 40.4	*
	Visible	0.007	0.054	0.900	0.000	-	ns
A3713	Invisible	-0.263	0.024	< 0.001	0.241	112.8 ± 14.5	***
	All data	-0.244	0.013	< 0.001	0.189	115.7 ± 8.2	***
	Visible	-0.248	0.026	< 0.001	0.210	125.2 ± 18.8	***
A3716	Invisible	0.188	0.058	0.001	0.042	106.4 ± 46.2	**
	All data	0.040	0.018	0.027	0.004	103.2 ± 66.1	*
	Visible	-0.024	0.027	0.376	0.002	112.8 ± 161.7	ns
A3717	Invisible	-0.010	0.027	0.719	0.000	-	ns
	All data	0.012	0.017	0.480	0.000	-	ns
	Visible	0.089	0.044	0.043	0.011	130.1 ± 77.6	*
A3723	Invisible	0.133	0.038	< 0.001	0.027	127.6 ± 43.2	***
	All data	-0.009	0.023	0.682	0.000	-	ns
	Visible	-0.153	0.032	< 0.001	0.030	80.1 ± 27.3	***
A3728	Invisible	-0.191	0.043	< 0.001	0.057	25.1 ± 19.6	***
	All data	-0.099	0.024	< 0.001	0.014	21.2 ± 26.1	***
	Visible	-0.076	0.084	0.365	0.006	116.5 ± 170.9	ns
A3730	Invisible	-0.061	0.026	0.020	0.017	88.1 ± 63.3	*
	All data	-0.046	0.011	< 0.001	0.012	66.4 ± 26.9	***
	Visible	-0.031	0.022	0.169	0.004	73.8 ± 77.1	ns

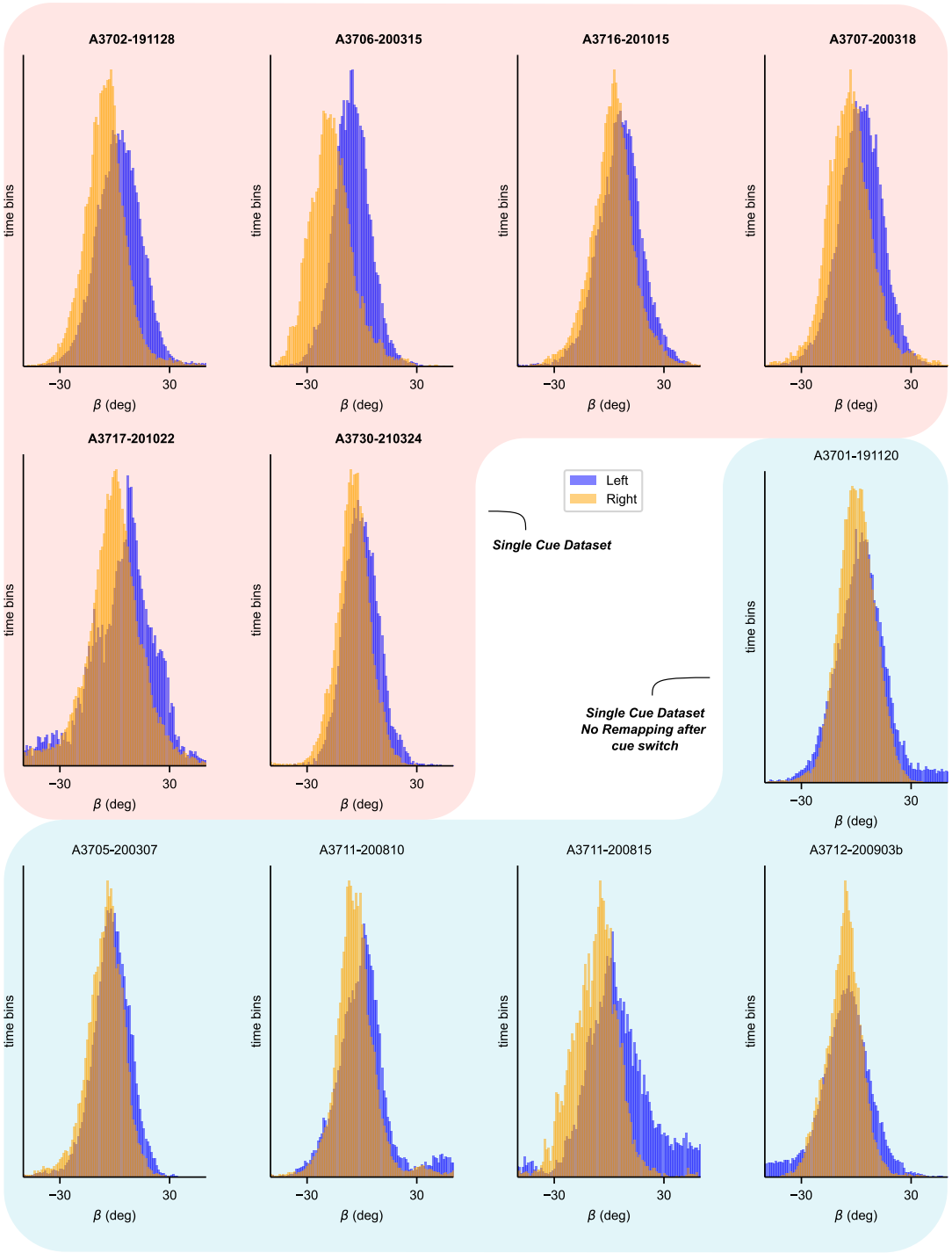

Figure 8: **Decoding error histogram split by left and right region in environment for single cue datasets.** Red background color indicates the six original sessions. Blue background color indicates the five additional sessions, where there was no observed remapping after cue switching.

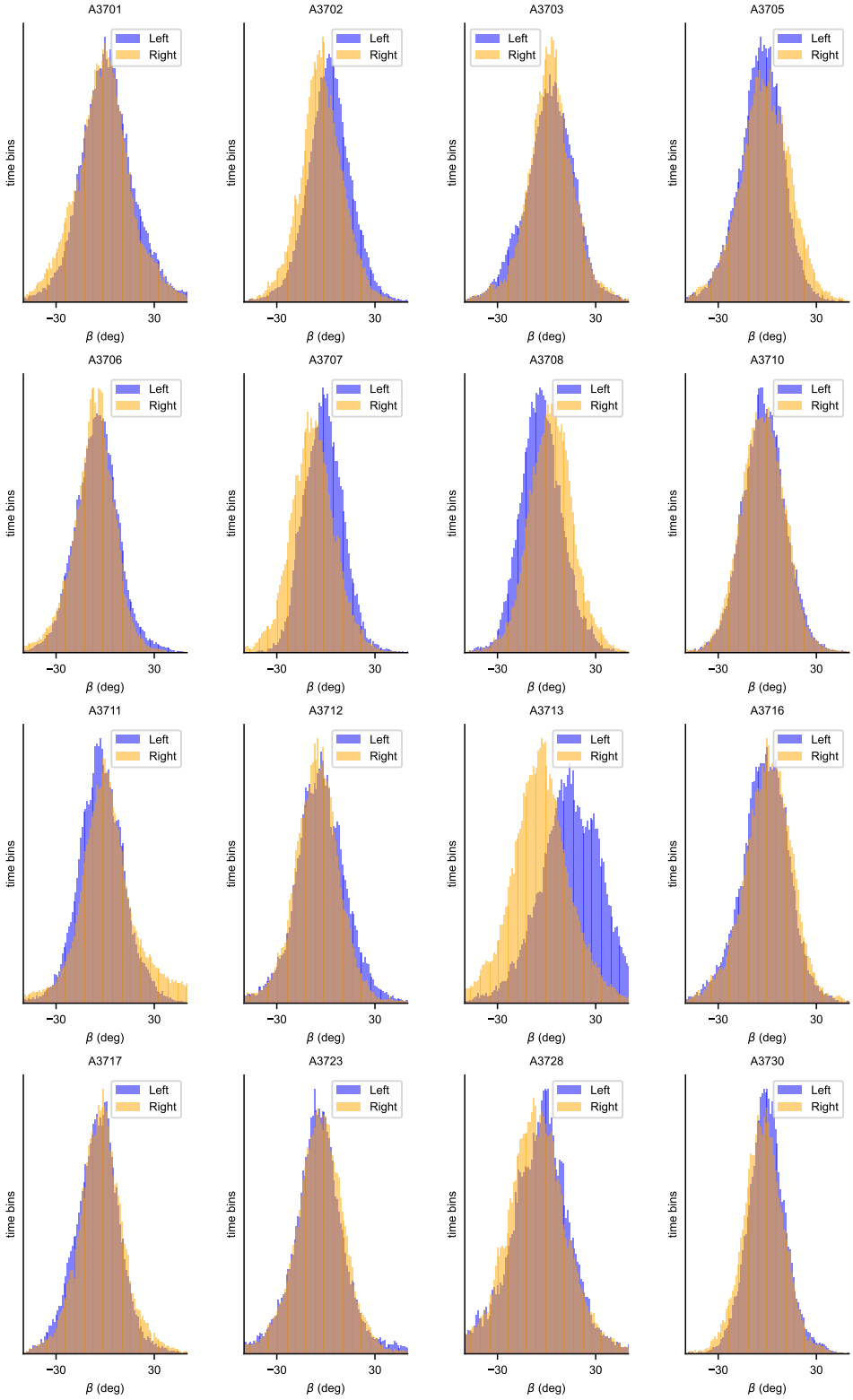

Figure 9: **Decoding error histogram split by left and right region in environment for multi cue dataset.**

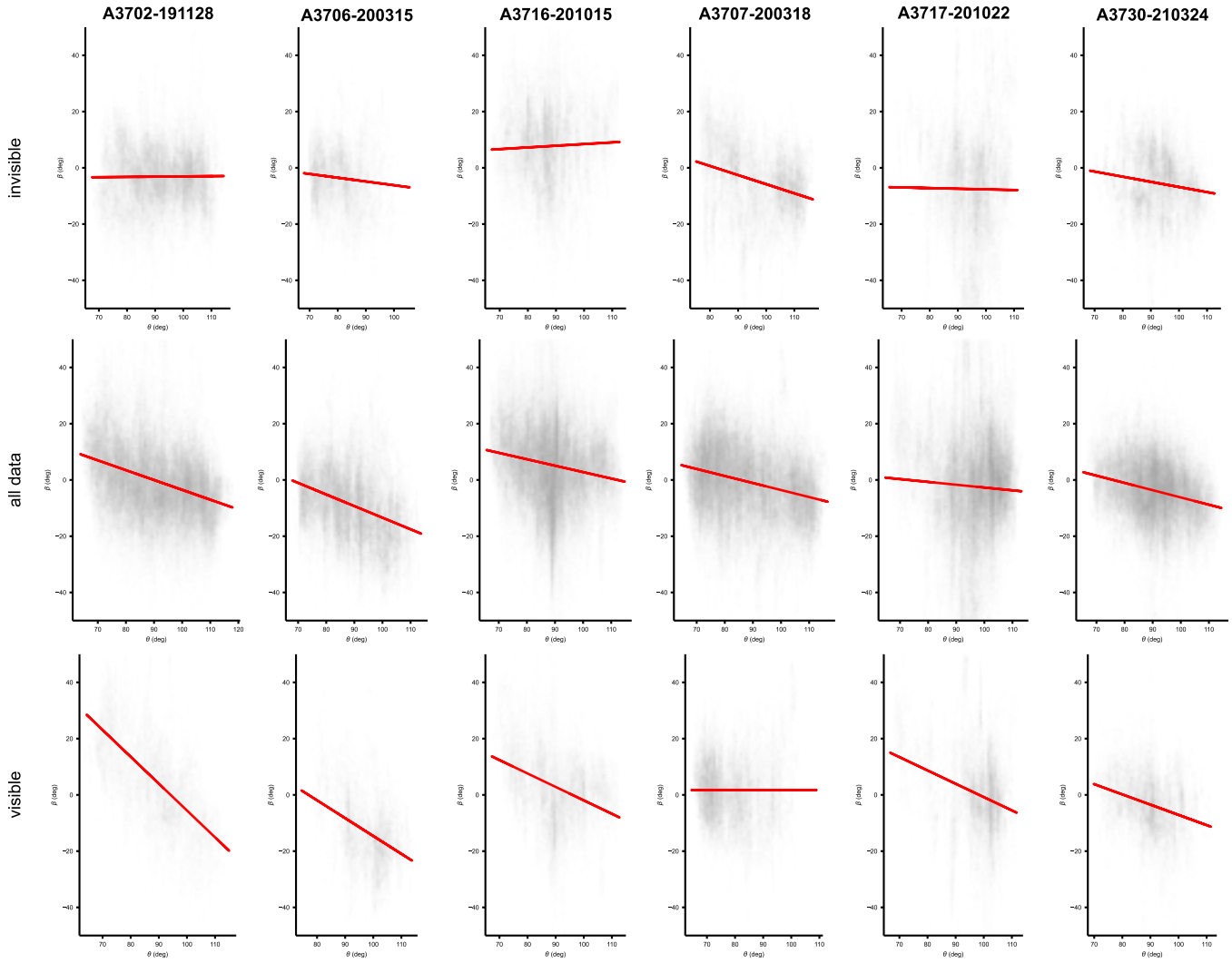

Figure 10: **Linear regression slopes for the single cue dataset in the invisible, all data, and visible conditions.**

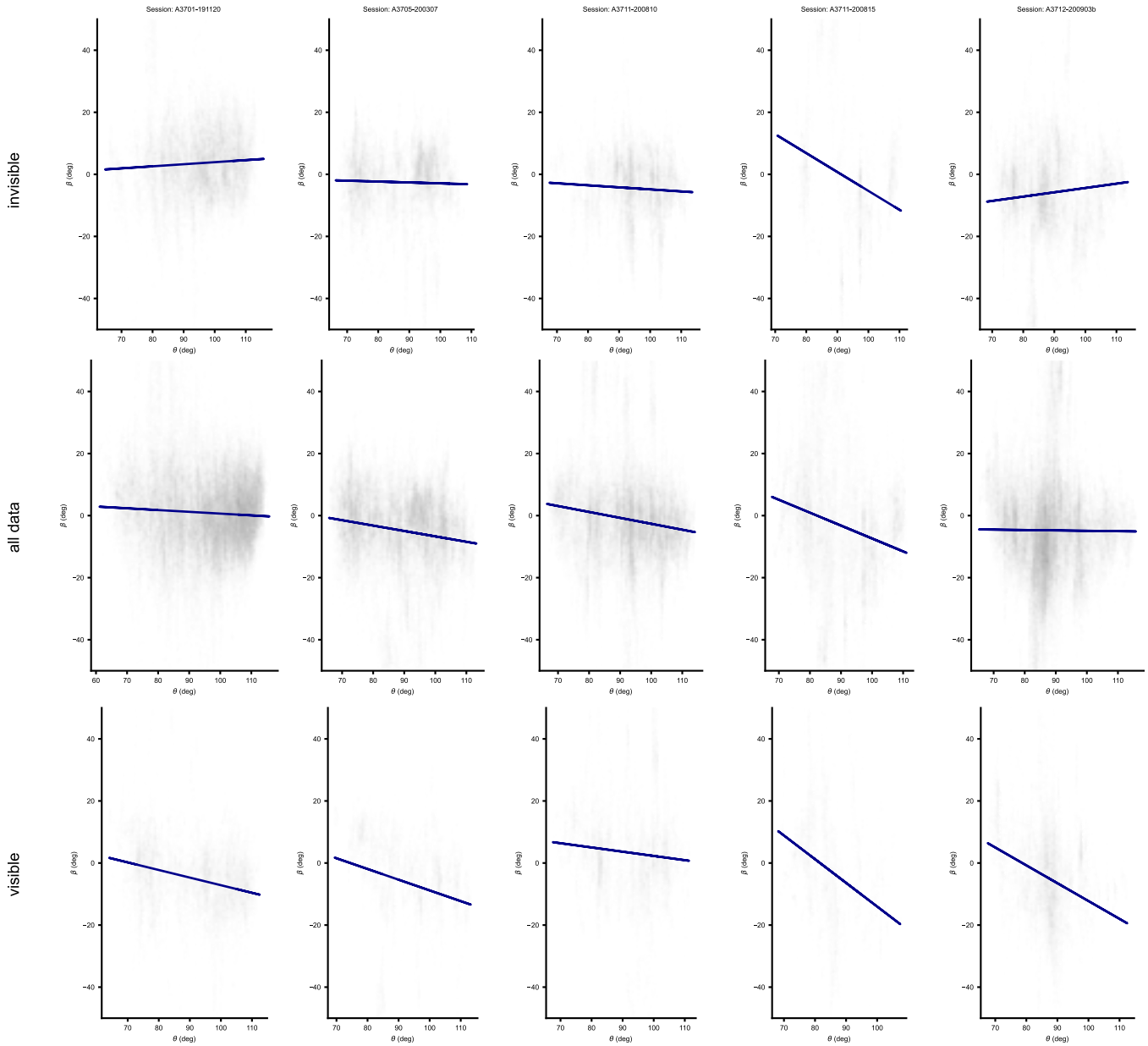

Figure 11: **Linear regression slopes for the single cue dataset with the sessions that do not show remapping in the invisible, all data, and visible conditions.**

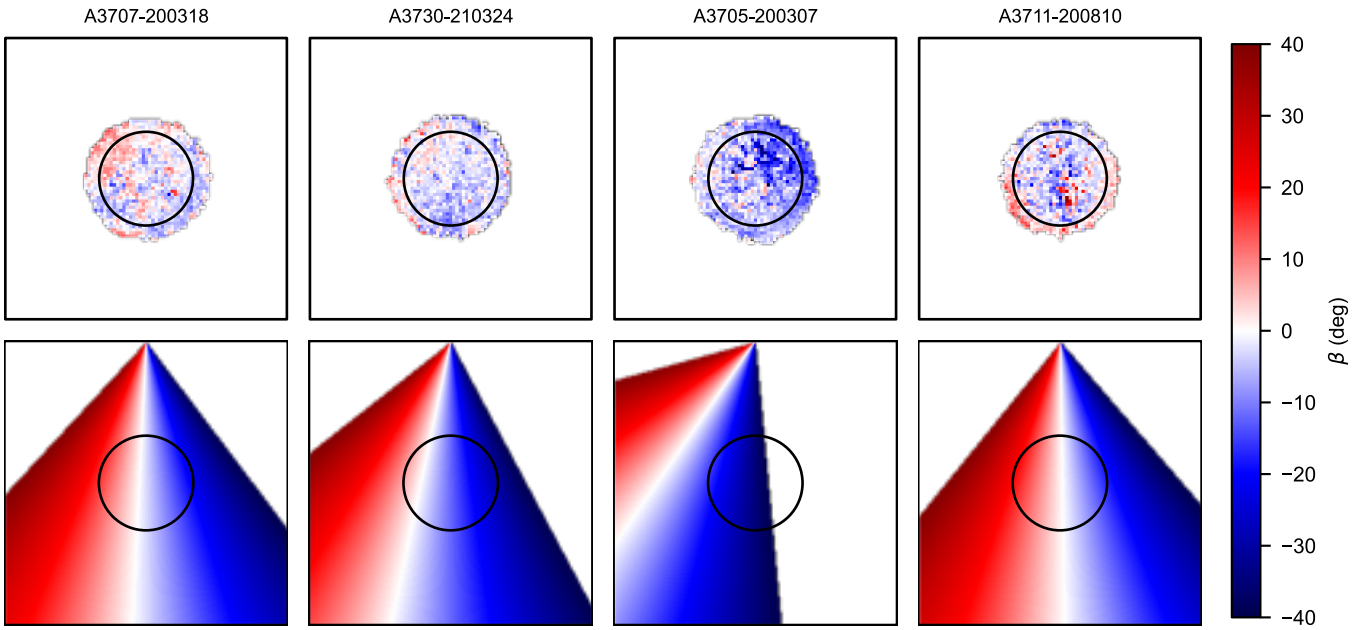

Figure 12: **Heatmap of measured parallax across space.** Same as Fig. 4, but for the additionaal 4 sessions of the anchoring angle analysis.

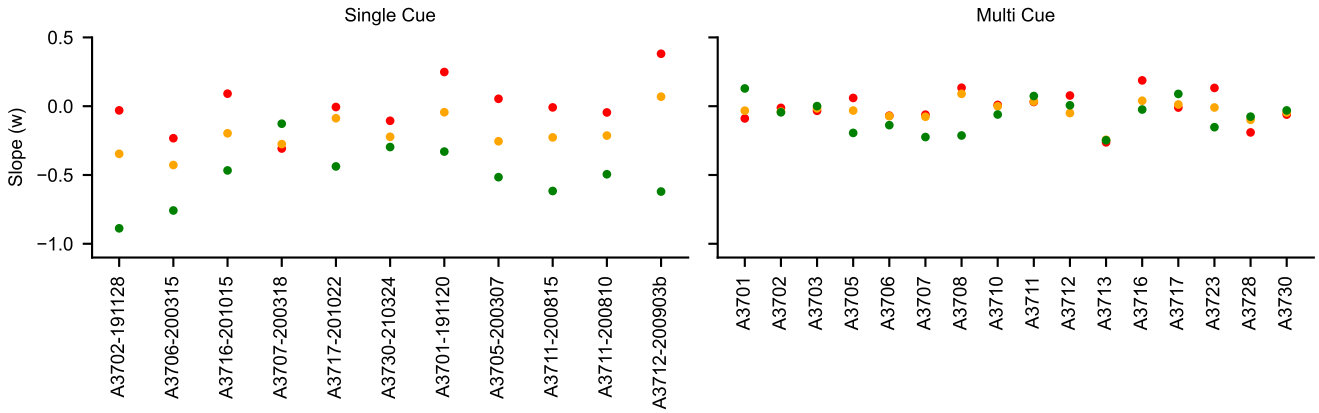

Figure 13: **Scatter plot of all measured slopes.** Slopes measured for all sessions in all three conditions (cue invisible (red), all data (orange), and cue visible (green)). Shown for all sessions in the single cue dataset (left) and multi cue dataset (right).

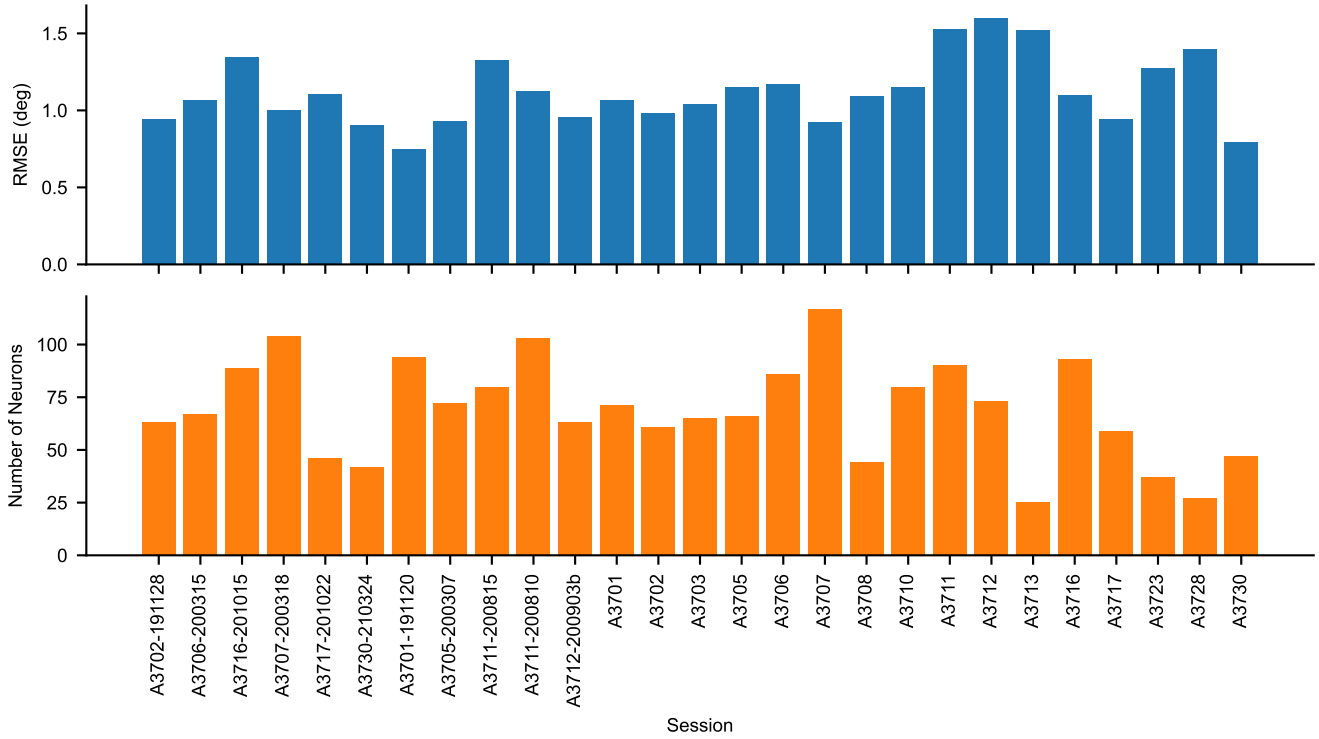

Figure 14: **Mean decoding error and number of neurons per session. (a)**: Bars show the root mean squared error between the tracked and decoded head direction. Switch periods and other rejected periods due to tracking errors are excluded from this data. **(b)**: Number of neurons recorded in each session.